Statistical linkage of daily precipitation in Switzerland to atmospheric circulation and temperature

Theo Brandsma*, T. Adri Buishand

Royal Netherlands Meteorological Institute (KNMI), P.O. Box 201, 3730 AE, De Bilt, The Netherlands

Abstract

The daily precipitation of Bern, Neuchâtel and Payerne in Switzerland is statistically linked to atmospheric circulation and temperature. For all three stations, there is a marked increase of the mean precipitation amount with increasing temperature for wet days with temperatures between −5 and 20°C. The amount of precipitation is also controlled by the direction and strength of the atmospheric flow. To take these dependencies into account, the daily precipitation amounts are modelled as a function of temperature and strength of the flow for three categories of flow direction. Both parametric and nonparametric techniques from the statistical literature on generalized linear models are applied. The nonparametric technique is a helpful tool for the selection and evaluation of parametric models. The non-linear effects of temperature and strength of the flow on the amount of precipitation are described by natural cubic splines and piecewise linear functions. The use of the modelled relationships for climate-change scenario production is discussed. © 1997 Elsevier Science B.V.

1. Introduction

General Circulation Models (GCMs) have been used to predict future climate conditions resulting from the increase of greenhouse gases in the atmosphere. Because of their coarse resolution and simplified physics, these models are unable to produce realistic precipitation scenarios needed for the assessment of the hydrological impact of climate change. One attempt to improve the representation of precipitation characteristics in the model simulations is to nest a Regional Climate Model (RegCM) within the GCM. RegCMs have a grid spacing of about 50 km (Giorgi et al., 1994; Jones et al., 1995). Because of computational restrictions, today the run length of the RegCM simulations does not exceed 10 years, which is actually too short for hydrological impact studies. In

* Tel.: +31 30 220 6693; fax: +31 30 221 0407; e-mail: brandsma@knmi.nl

comparison with GCMs, RegCMs produce more realistic regional details of surface climate as forced by topography, large lake systems or narrow land masses. However, the difference in seasonal precipitation between the control runs and the observed values (bias) in present-day simulations of regional climate is still too large to yield a high level of confidence in simulated climate change scenarios. The simulated changes in seasonal precipitation owing to doubling CO_2 concentrations, are generally the same or smaller than the precipitation biases (Kattenberg et al., 1996).

Stochastic simulation of time series has been a popular tool for deriving precipitation scenarios indirectly. The two main approaches are: (1) adjusting the parameters in a stochastic precipitation model in a manner consistent with the GCM predicted changes in mean precipitation (Burlando and Rosso, 1991; Cole et al., 1991; Wilks, 1992); and (2) driving a stochastic precipitation model with the GCM results for the large-scale atmospheric circulation (Bárdossy and Plate, 1992; Hughes et al., 1993; Zorita et al., 1995). A weakness of the first approach is that it relies on the GCM predicted changes in mean precipitation, which are known to be unreliable. The second approach assumes that the GCMs realistically reproduce the large-scale features of the upper air and that the change in precipitation is solely a result of changes in the large-scale circulation. Consequently, the direct effect of the greenhouse-gas-induced higher temperatures on precipitation is not taken into account.

Matyasovszky et al. (1993) proposed a modification of the latter approach, based on their experience with upper air characteristics in a simulation with the Canadian Climate Centre GCM. They observed that the patterns of the 500 hPa field over their region of interest were similar in the $1 \times CO_2$ and $2 \times CO_2$ cases and that there was a significant increase in the heights of this pressure level for the $2 \times CO_2$ case. The latter is related to the higher temperatures in the lower atmosphere. To generate daily precipitation sequences for a $2 \times CO_2$ case, they used the changes in the average height of the 500 hPa level to adjust the parameters of the daily precipitation distribution in a modified version of the model of Bárdossy and Plate (1992). The other characteristics of the circulation were assumed to remain the same. In this paper, we follow a quite different approach by taking the relationship between precipitation and temperature (P–T relationship) as a basis for precipitation scenario construction. Buishand and Klein Tank (1996) studied this relationship in order to derive precipitation scenarios for De Bilt, The Netherlands. In the present paper, we extend their work by including information about the direction and strength of the atmospheric flow and by using more flexible statistical models to describe P–T relationships in order to obtain precipitation scenarios for western Switzerland. Data from the stations Bern, Neuchâtel and Payerne are analysed for this purpose. As a result, a temperature and flow-direction-dependent scaling-factor is given that can be used to derive a scenario of daily precipitation for the case of a spatially homogeneous warming. The research in this paper is part of the EC-project POPSICLE (Production of Precipitation Scenarios for Impact Assessment of Climate Change in Europe).

The paper is organised as follows. In Section 2, we first present empirical P–T relationships for Bern, Neuchâtel and Payerne. Then we show that the P–T relationships depend on the direction of the atmospheric flow and that the strength of the flow is a necessary additional explanatory variable. Section 3 deals with statistical methods for linking the precipitation to the predictor variables. In that section, a survey is given of techniques that

have been developed for data analysis with generalized linear models (McCullagh and Nelder, 1989). A nonparametric smoothing technique is introduced to explore a relationship and to test the adequacy of fitted parametric models. In Section 4, we present the results for the three Swiss stations. The model choice is discussed in detail. The fitted parametric model for Bern is used in Section 5 to estimate the change in mean precipitation for the case of a spatially homogeneous warming. A short evaluation of our approach is also given in that section. Section 6 contains the conclusions.

2. Description and analysis of data

In this section, we first give some background on the precipitation and temperature data used in this study, then, empirical relationships between precipitation and temperature are presented for wet days, where a wet day refers to a day with precipitation greater than or equal to 0.3 mm. The influence of the direction and strength of the flow is discussed. The need for eliminating seasonal variation is questioned.

2.1. Data description and empirical P–T relationships

2.1.1. Precipitation and temperature data

The locations of the three stations Bern, Neuchâtel and Payerne are shown in Fig. 1. Bern and Payerne are situated in the Swiss Midland and Neuchâtel is situated along the south-easterly foothills of the Jura Mountains that border the Swiss Midland. According to Schüepp and Schirmer (1977), the entire area of the Midland has the maximum precipitation in summer, mainly in the form of pre- or post-frontal showers or thunderstorms, whereas in winter frontal precipitation predominates, modified by upslope or lee effects.
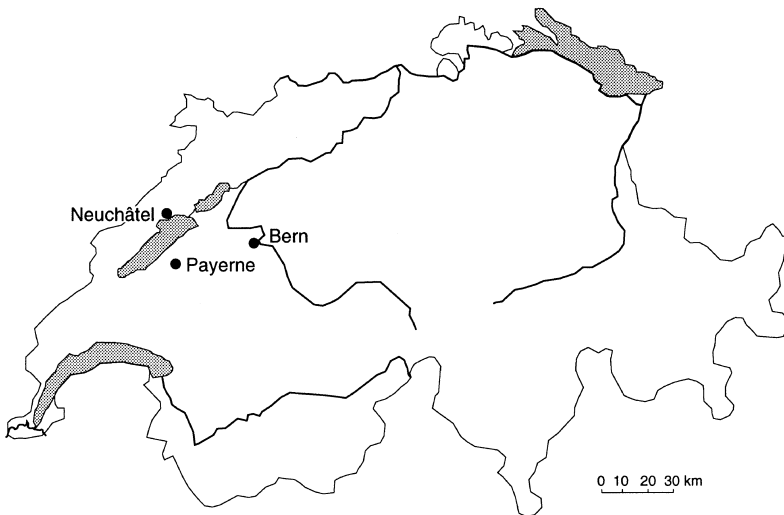

Fig. 1. Site map.

The mean wet-day precipitation amounts vary from about 5 mm in winter to nearly 9 mm in July and August. The characteristics of precipitation for Neuchâtel are quite similar to those for the Swiss Midland.

For all three stations, daily precipitation data were obtained for the period 1901–1993. Daily temperature data for that period were available for Bern and Neuchâtel, but for Payerne only data for 1978–1993 were available. Because the spatial variability of temperature is small, we have used the temperature series of Bern, corrected for the difference in station altitude, as a substitute for the temperature at Payerne. The corrections have been obtained by adding the difference between the mean monthly temperatures of Payerne and Bern for the period 1978–1993 to the complete daily temperature series of Bern. The corrections were rather small and ranged between 0.31°C for the months of May and June and 0.61°C for the month of January. Some information about the three stations is given in Table 1.

2.1.2. Empirical P–T relationships

Temperature determines the maximum moisture content of the air. The strength of convection is also controlled by temperature. Because of these factors, there is a link between precipitation and near-surface temperature. The annual cycle in the mean wet-day precipitation amounts in western Switzerland is mainly due to this temperature dependence.

Fig. 2 presents, for Bern, Neuchâtel and Payerne, the mean precipitation amounts at various temperatures. Temperature and precipitation in this figure are averages on wet days for preselected temperature intervals of 2°C. However, classes with less than six wet days have been combined with the adjoining classes.

The $P–T$ diagrams of the three stations have much in common. At temperatures of less than 8°C, when frontal precipitation predominates, there is a rapid increase in the mean precipitation amounts with increasing temperature. At 10°C, there is a small dip in the mean precipitation amounts for all three stations. From 10°C to about 15°C there is again an increase in the mean precipitation amounts with increasing temperature. For temperatures greater than 15°C the standard errors of the mean precipitation amounts start to increase and the differences in the shape of the $P–T$ relationships between the three stations become more pronounced. In particular for Bern and Neuchâtel there is even a decrease for temperatures greater than 20°C.

Fig. 3 shows, for Bern, the dependence between daily precipitation and temperature after removing the annual cycles in the mean wet-day temperature and precipitation. Here,

Table 1
Characteristics of stations that have been used in the study (mean annual values for the period 1901–1993)

Station	Altitude (m above m.s.l.)	Mean annual temperature (°C)	Mean annual precipitation (mm)
Bern	572	8.7	1009
Neuchâtel	489	9.6	975
Payerne	441	9.1 [a]	895

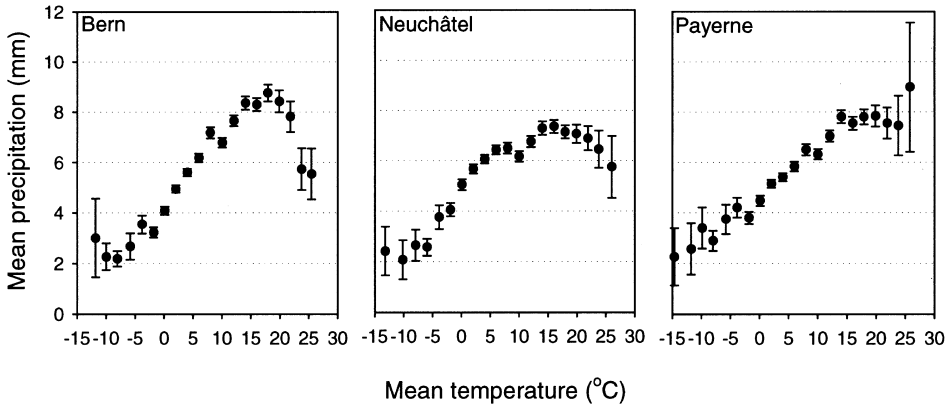[a] Estimated from a short local record and the long-term Bern data (see text).

Fig. 2. Relationship between daily mean precipitation and daily mean temperature for wet days (0.3 mm or more) at Bern, Neuchâtel and Payerne for the period 1901–1993. The error bars give the standard error of the mean precipitation within each class. The total number of wet days for the three stations is 14062, 14147 and 13173, respectively.

daily precipitation amounts were divided by their long-term monthly means (relative daily precipitation anomalies P') and the long-term monthly mean temperatures were subtracted from the daily temperatures (daily temperature anomalies T'). The left panel in Fig. 3 shows the mean relative daily precipitation anomaly $\bar{P}'$ as a function of T' over the whole year. For most wet days T' is between −5°C and +5°C. In that temperature anomaly range there is an almost linear increase in $\bar{P}'$ with increasing T' (about 4.5% per °C). There is, however, no increase at high T'. The middle and right panels in Fig. 3 give the corresponding diagrams for the winter half of the year (October–March) and the summer half of the year (April–September). There are marked differences between these two diagrams.
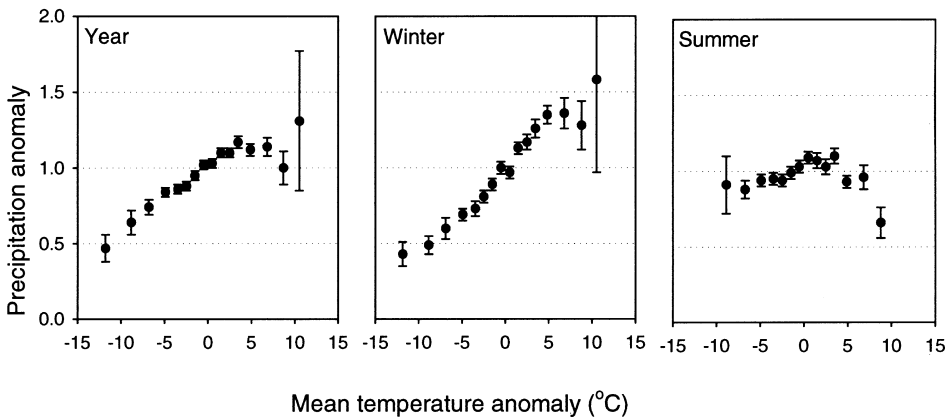

Fig. 3. Mean relative precipitation anomaly as a function of the daily temperature anomaly for wet days (0.3 mm or more) at Bern for the whole year, the winter half of the year and the summer half of the year for the period 1901–1993. Anomalies are with respect to the long-term monthly mean wet-day precipitation amounts and temperatures. The error bars give the standard error of the mean precipitation anomaly within each class.

The relatively large change of $\bar{P}'$ with T' for the winter half of the year (about 7% per °C) agrees with the observed increase in the mean wet-day precipitation amounts at low and moderate temperatures in Fig. 2. Also, the diminishing of that increase at high temperatures is consistent with the relatively small change in $\bar{P}'$ for positive T' in the summer half of the year.

2.2. Atmospheric circulation and the P–T relationship

The atmospheric circulation is an important factor for the amount of precipitation. Because of this link, the changes in the mean wet-day precipitation amounts shown in Fig. 2 may not be representative of the true temperature effect. Daily mean sea-level pressure (MSLP) data on a $5° \times 10°$ grid from the UK Meteorological Office, covering the whole 1901–1993 period, were used to account for the atmospheric circulation. We centred the grid over Switzerland (see Fig. 4) and calculated, for each day, the direction of the flow, the strength of the flow F, and the total shear vorticity Z. The latter is a measure of the rotation of the atmosphere. Positive vorticity corresponds to a low pressure area (cyclonic) and negative vorticity corresponds to a high pressure area (anti-cyclonic). The derivation of the air-flow indicators is explained in Jones et al. (1993).

For the Swiss data it turned out that the direction and strength of the flow had a stronger impact than vorticity on the wet-day precipitation amounts. To incorporate the direction of the flow, we plotted the P–T diagrams for each 45° sector of flow direction. Sectors with identical plots were grouped. This resulted in a classification of three categories of flow
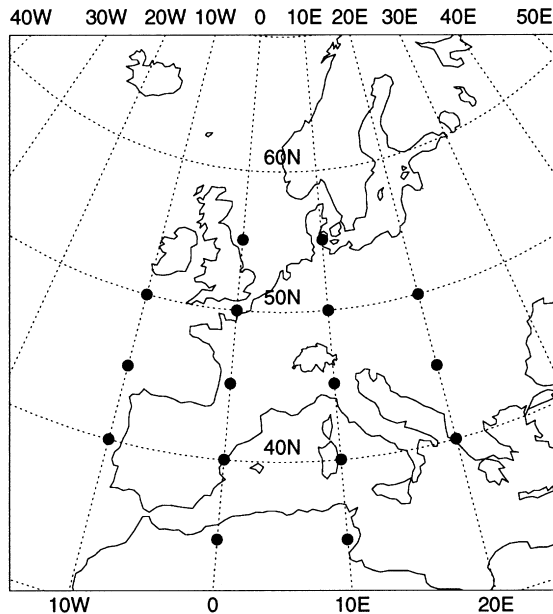

Fig. 4. Grid points of mean sea-level pressure used for the calculation of the air-flow indicators over Switzerland. Switzerland is situated at about 47N–8E.

direction: (1) N/NE; (2) E/SE/S; and (3) SW/W/NW. Most rain (on average 64% for the three stations) comes from the SW/W/NW category. The probability of precipitation for the E/SE/S category is relatively small owing to a screening influence of the Alps. For Bern the $P-T$ relationships for the three categories are presented in Fig. 5. The figure shows that for most temperatures, the mean precipitation amounts for the SW/W/NW category are 1–2 mm higher than for the other two categories. For the E/SE/S category the mean daily precipitation amounts show the least variation with temperature. A strong increase in the mean daily precipitation with increasing temperature is found for the N/NE category.

The strength of the atmospheric flow F influences the enhancement of precipitation in hilly and mountainous areas by orographic lifting (Weston and Roy, 1994; Brown, 1995). For the Swiss stations, F has the strongest effect in the SW/W/NW category. This is illustrated in Fig. 6, which gives the mean wet-day precipitation amounts in distinct classes of T and F for Bern. The enhancement of precipitation with increasing strength of the flow is apparent from this figure. Fig. 6 also shows that precipitation at high temperatures (summer showers) is not associated with strong winds.

2.3. Seasonal variation

Like temperature, the strength of the flow exhibits a clear annual cycle. For wet days, the mean of F in winter is about twice as large as it is in summer. Besides the annual cycles in the means of T and F, their relationship with precipitation varies over the year. The annual cycle in the monthly mean wet-day precipitation amounts, assuming a constant relationship, might, therefore, differ from the observed annual cycle. In the case of a constant $P-T$ relationship, the expected monthly means are easily obtained by replacing the observed precipitation amount of each wet day by the mean precipitation amount in the appropriate temperature class (dots in Fig. 2). For a constant relationship with T and F, the
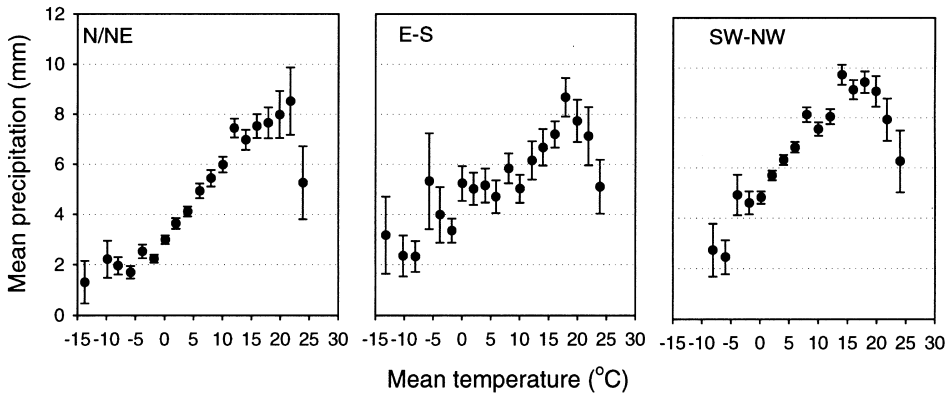

Fig. 5. Relationship between daily mean precipitation and daily mean temperature for wet days (0.3 mm or more) at Bern for the period 1901–1993 for three categories of flow direction: (1) N/NE; (2) E/SE/S; and (3) SW/W/NW. The error bars give the standard error of the mean precipitation within each class. The total number of wet days for the three categories of flow direction is 4617, 1716 and 7729, respectively.
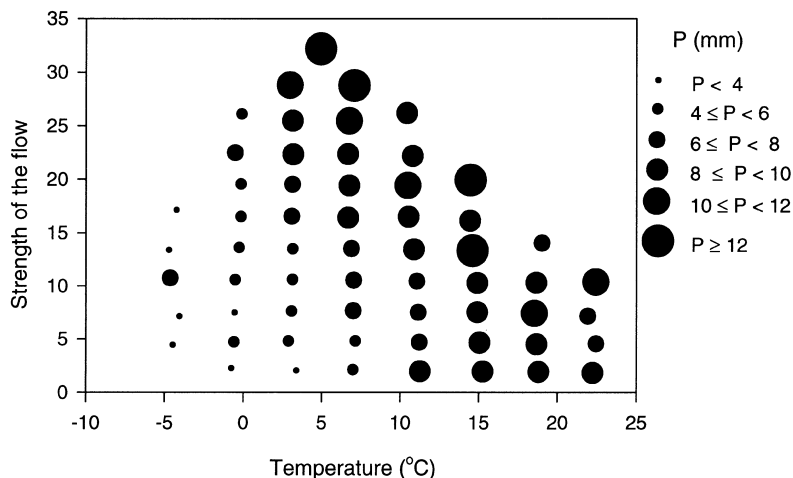
Fig. 6. Relationship between daily mean precipitation, temperature and strength of the flow for wet days (0.3 mm or more) at Bern (1901–1993) for the SW/W/NW category. The radii of the circles are directly proportional to the magnitude of the mean precipitation amounts; flow units are geostrophic, expressed as hPa per $10°$ latitude at $45°$N (1 unit is equivalent to 0.87 m s^{-1}).

expected monthly means follow similarly from the mean wet-day precipitation amounts in the various classes of these predictor variables. Fig. 7 compares the observed monthly mean wet-day precipitation amounts for Bern with those for a constant relationship with T and for a constant relationship with T and F within each category of flow direction. In both cases, the mean wet-day precipitation amount is underestimated in July and August and overestimated in spring. A similar discrepancy, though somewhat larger in magnitude, was
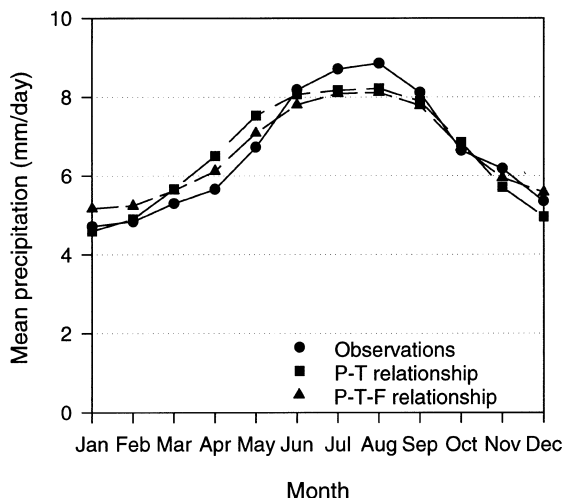

Fig. 7. Comparison between the observed monthly mean wet-day precipitation amounts for Bern (1901–1993) and the expected monthly means for constant $P-T$ and $P-T-F$ relationships over the year. Different $P-T-F$ relationships are assumed for each of the three categories of flow direction N/NE, E/SE/S and SW/W/NW.

observed by Klein Tank and Buishand (1993) for De Bilt. Additional predictor variables would be needed to obtain a better description of the annual cycle of the mean wet-day precipitation amounts. Plausible variables were, however, not available in this study.

Fig. 3 already showed quite different relationships for the anomalies in the winter and summer halves of the year. Seasonal variation, thus, cannot simply be removed by analysing anomalies instead of the original data. Working with anomalies of T and F is also rather unnatural because factors like the maximum atmospheric moisture content and orographic enhancement are actually related to T and F themselves. Part of the seasonal variation in the anomalies is due to nonlinearities in the effects of T and F. A satisfactory treatment of seasonal variation, in fact, needs a separate analysis for each season. This leads, however, to a considerable increase in the number of parameters.

The constant relationship with T and F explains a large part of the annual cycle in the mean wet-day precipitation amounts. It also reasonably describes the relatively strong change in the mean wet-day precipitation amounts with increasing temperature during the winter season and the relatively strong effect of F during that season. Seasonal variation in the relationship with T and F was, therefore, ignored in the statistical analysis.

3. Statistical modelling

The statistical modelling of relationships like those presented in Figs 2, 5 and 6 is not a trivial problem. The main difficulty is that the standard deviation of daily precipitation often tends to be large in situations where the mean amount is large. The statistical techniques that deal with such data have shown a rapid development during the past 20 years. In this section, we give the necessary background for the applications to the Swiss precipitation data. For ease of exposition, the case of a single predictor variable (temperature) is addressed first. Both parametric and nonparametric methods are discussed. The extension to more than one predictor variable (both temperature and strength of the flow) is examined at the end of this section.

3.1. Parametric models for the P–T relationship

3.1.1. Model description
For the statistical analysis, it is useful to represent the amount of precipitation P on a wet day with temperature T as:

$$P = \exp[g(T)] + \epsilon \tag{1}$$

where $g(T)$ is a function of T and ϵ is a random error with zero mean. The first term on the right-hand side gives the expected value, μ, of P:

$$\mu = E(P) = \exp[g(T)] \tag{2}$$

The change of the mean precipitation amount with T is thus determined by the function $g(T)$. For the linear model:

$$g(T) = a + bT \tag{3}$$

the mean increases exponentially with increasing T. From the diagrams in Section 2, it is clear that more general functions are needed. Piecewise polynomials can be used to describe complex relationships. For the P–T relationship at De Bilt (The Netherlands), Buishand and Klein Tank (1996) considered the following function:

$$g(T) = \begin{cases} a+bT & T \le s_1 \\ a+bT+c(T-s_1)^2+d(T-s_1)^3 & s_1 < T \le s_2 \\ a+bT+c(s_2-s_1)(2T-s_2-s_1) & \\ \quad +d(s_2-s_1)^2(3T-2s_2-s_1) & T > s_2 \end{cases} \tag{4}$$

where s_1 and s_2 are two pre-chosen knots. The function $g(T)$ is, thus, linear in the regions beyond these knots. Linearity is assumed in these regions to avoid large standard errors and rapid changes of the fitted values at the ends of the temperature range. The polynomial pieces fit together at the knots in such a way that $g(T)$ and its first derivative are continuous everywhere. The second derivative of $g(T)$ has, however, a discontinuity at the knots s_1 and s_2.

In this study, natural cubic splines are considered. A natural cubic spline (NCS) with knots $s_1, \ldots, s_q$ is a separate polynomial for each of the intervals $(s_1, s_2), \ldots, (s_{q-1}, s_q)$ and is linear outside (s_1, s_q). The different pieces are forced to join at these knots such that $g(T)$ itself and its first and second derivatives are continuous at each s_j and thus over the entire temperature range. These continuity constraints and the linearity for $T < s_1$ require that $g(T)$ is of the form:

$$g(T) = a+bT+\sum_{j=1}^{q} d_j \left(T-s_j\right)^3_+ \tag{5}$$

where $(T-s_j)_+ = \max(0, T-s_j)$. This equation contains $q+2$ parameters. Linearity for $T > s_q$ leads to the following two parameter constraints:

$$\begin{cases} d_1+d_2+\cdots+d_q=0 \\ d_1s_1+d_2s_2+\cdots+d_qs_q=0 \end{cases} \tag{6}$$

The total number of unknown parameters is, therefore, equal to the number of knots. For $q = 2$, Eq. (6) yields $d_1 = d_2 = 0$ and the NCS reduces to the linear model given by Eq. (3). Computer programmes for fitting natural cubic splines generally make use of the B-spline basis functions:

$$g(T) = \sum_{j=1}^{q} \theta_j B_j(T) \tag{7}$$

Each $B_j(T)$ is a non-negative piecewise cubic polynomial with only limited support: for $3 \le j \le q-2$ the function $B_j(T)$ is zero outside (s_{j-2}, s_{j+2}), whilst $B_1(T)$, $B_2(T)$, $B_{q-1}(T)$ and $B_q(T)$ are similar, but linear or constant outside (s_1, s_q). Further details about the natural B-spline basis can be found in Greville (1969).

The function $g(T)$ is linear in the unknown parameters a and b in Eq. (3) and $\theta_1, \theta_2, \ldots, \theta_q$ in Eq. (7). The model given by Eq. (1) is, however, non-linear in these parameters

because of the exponential function. Another complication is that the distribution of ϵ depends on T. For the precipitation amounts in Fig. 2, the standard deviation σ of P increases from about 5 mm at $T = 0°C$ to 10 mm at $T = 20°C$. The coefficient of variation $CV = \sigma/\mu$ shows less variation. Therefore it makes sense to consider CV rather than σ. The change of CV with temperature can simply be described by a linear relation:

$$CV = \alpha + \beta T \tag{8}$$

A consequence of the use of this relation is that the variance depends on the expected response, μ. We further assume that there is no correlation between the errors, ϵ, for successive wet days.

3.1.2. Fitting procedure

The situation where the expected response, μ, is a monotone function of a linear combination of unknown parameters and where the variance is a function of μ, is characteristic of generalized linear models and their extensions. These models are discussed in detail in McCullagh and Nelder (1989). An introduction to generalized linear models in hydrology can be found in Clarke (1994). Parameter estimation in these models is based on an iteratively-reweighted least-squares (IRLS) algorithm. The unknown coefficients in $g(T)$ can be estimated by an IRLS fit to the mean precipitation amounts in the various temperature classes (Buishand and Klein Tank, 1996). It can be shown that the IRLS procedure reduces to an iterative adjusted dependent variable regression.

Let n_k denote the number of wet days, $\bar{T}_k$ the mean temperature and $\bar{P}_k$ the mean precipitation amount for the kth temperature class ($k = 1, ..., K$). The adjusted dependent variable z_k is defined as:

$$z_k = \ln\mu_k + \frac{\bar{P}_k - \mu_k}{\mu_k} \quad k = 1, ..., K \tag{9}$$

where

$$\mu_k = \exp[g(\bar{T}_k)] \tag{10}$$

is the expected value of $\bar{P}_k$. The variable z_k is just the first-order Taylor expansion of $\ln(\bar{P}_k)$ about μ_k. The μ_k and z_k values are calculated after each iteration step, using the current estimates of the coefficients in $g(\bar{T}_k)$. Revised estimates are then obtained by a linear regression of z_k on the various temperature components of $g(\bar{T}_k)$ with weight ω_k. For the linear model given by Eq. (3) the model for z_k reads:

$$z_k = a + b\bar{T}_k + \eta_k \quad k = 1, ..., K \tag{11}$$

and for the NCS we have:

$$z_k = \theta_1 B_1(\bar{T}_k) + \cdots + \theta_q B_q(\bar{T}_k) + \eta_k \quad k = 1, ..., K \tag{12}$$

In both cases η_k is a random error with mean 0 and variance CV_k^2/n_k, with CV_k the coefficient of variation for the kth class, and $\omega_k = n_k/CV_k^2$. With the revised parameter estimates new values of μ_k and z_k can be computed, and the process is repeated until the relative change in the coefficients is small. The process is started with $\bar{P}_k$ as a first estimate of μ_k. Further details on the adjusted dependent variable regression are given in Buishand

and Klein Tank (1996). In this paper, the S-PLUS software (see e.g. Chambers and Hastie, 1993) was used to obtain parameter estimates and to assess the adequacy of the fit.

The weights in the adjusted dependent variable regression need an estimate of the coefficients of variation CV_k. These are derived from Eq. (8). The parameters α and β in that equation are obtained from a weighted least-squares fit (with weight n_k) to the sample coefficient of variation in the various classes.

3.1.3. Testing goodness of fit and model comparison

Because the number of wet days is large, it is quite reasonable to treat the CV_k values from Eq. (8) as known constants. For the mean precipitation amounts, the following scaled log quasi-likelihood can then be defined:

$$Q(\boldsymbol{\theta}) = -\frac{1}{CV_k^2} \sum_{k=1}^{K} n_k \left[\frac{\bar{P}_k}{\mu_k(\boldsymbol{\theta})} + \ln \mu_k(\boldsymbol{\theta}) \right] \tag{13}$$

with $\boldsymbol{\theta}$ the vector of unknown coefficients in $g(T)$. The IRLS procedure maximises $Q(\boldsymbol{\theta})$ with respect to $\boldsymbol{\theta}$. The scaled log quasi-likelihood can be used to test the significance of the various terms in $g(T)$ in the same way as a log likelihood (McCullagh, 1986). It also provides a goodness-of-fit statistic for testing the adequacy of the fitted model.

Let H_0 and H_1 be two nested hypotheses about $g(T)$ with p and $q > p$ coefficients, respectively. For instance, under the null hypothesis H_0 we may assume that $g(T)$ is linear ($p = 2$) as given by Eq. (3) and under H_1 we assume that $g(T)$ is an NCS with $q > 2$ knots. Then a quasi-likelihood-ratio statistic can be obtained as:

$$QLR = 2[Q(\hat{\boldsymbol{\theta}}_1) - Q(\hat{\boldsymbol{\theta}}_0)] \tag{14}$$

with $\hat{\boldsymbol{\theta}}_0$ and $\hat{\boldsymbol{\theta}}_1$ the vectors of parameter estimates under H_0 and H_1, respectively. Under H_0, QLR has an asymptotic chi-squared distribution with $q - p$ degrees of freedom.

A perfect fit to the mean precipitation amounts is obtained if we take $\mu_k = \bar{P}_k$, $k = 1, \ldots, K$. This is in fact a K parameter model. The scaled log quasi-likelihood is then maximal:

$$Q_{\max} = -\frac{1}{CV_k^2} \sum_{k=1}^{K} n_k [1 + \ln \bar{P}_k] \tag{15}$$

For the model under investigation the μ_k values are estimated as $\hat{\mu}_k = \mu_k(\hat{\boldsymbol{\theta}})$ and the maximised $Q(\boldsymbol{\theta})$ is $Q(\hat{\boldsymbol{\theta}})$. The difference between $Q_{\max}$ and $Q(\hat{\boldsymbol{\theta}})$ is a measure of the goodness of fit. The scaled deviance:

$$D(\hat{\boldsymbol{\theta}}) = \frac{2}{CV_k^2} \sum_{k=1}^{K} n_k \left[\frac{\bar{P}_k - \mu_k(\hat{\boldsymbol{\theta}})}{\mu_k(\hat{\boldsymbol{\theta}})} - \ln \left(\frac{\bar{P}_k}{\mu_k(\hat{\boldsymbol{\theta}})} \right) \right] \tag{16}$$

has under H_0 a chi-squared distribution with $K - p$ degrees of freedom where p is the number of parameters under H_0.

An alternative goodness-of-fit test based on the generalized Pearson x^2 statistic was considered in Buishand and Klein Tank (1996). This statistic is just the first-order Taylor

approximation of $D(\hat{\boldsymbol{\theta}})$. It should be noted further that the *QLR* statistic in Eq. (14) can be rewritten as the difference between the scaled deviances under H_0 and H_1:

$$QLR = D(\hat{\boldsymbol{\theta}}_0) - D(\hat{\boldsymbol{\theta}}_1) \tag{17}$$

Besides the *QLR* statistic the Akaike-information criterion (*AIC*) can be used to select the number of parameters. The *AIC* statistic is defined by (Hastie and Tibshirani, 1990):

$$AIC = D(\hat{\boldsymbol{\theta}}) + 2q \tag{18}$$

with q denoting the number of parameters in the model. Inclusion of an extra parameter reduces $D(\hat{\boldsymbol{\theta}})$, but leads to an increase of the second term on the right-hand side of Eq. (18). That term can be thought of as a penalty for heavily parameterized models. The model for which *AIC* is smallest is selected. A *QLR* test at the 5% level is a more severe criterion for the inclusion of a small number of additional parameters than the *AIC* (Hastie and Tibshirani, 1990).

3.2. Nonparametric modelling of the P–T relationship

In the nonparametric approach $g(T)$ is estimated without reference to a specific mathematical form. The value of $g(T)$ at a certain temperature T_0 is estimated from a local approximation of $g(T)$ using only data from an interval around T_0. This can be done in different ways. In this paper, we use the so-called locally weighted running-line or loess smoother owing to Cleveland (1979). For each T_0 the linear model in Eq. (3) is fitted in a neighbourhood $N(T_0)$ around T_0 and $g(T_0)$ is then estimated as the fitted value at T_0:

$$\hat{g}(T_0) = \hat{a}(T_0) + \hat{b}(T_0)T_0 \tag{19}$$

Here $\hat{a}(T_0)$ and $\hat{b}(T_0)$ denote the estimates of the coefficients a and b from the local fit. These estimates are obtained from an iterative process using the adjusted dependent variable z_k given by Eq. (11). The weights in the adjusted dependent variable regression now depend on both $\mathrm{var}(\eta_k)$ and the distance d_k of $\bar{T}_k$ to the target point T_0. To account for the latter, a tricube weight function is introduced:

$$W_k = \left[1 - \left(\frac{d_k}{d_{\max}} \right)^3 \right]^3 \quad k = 1, \ \ldots, \ r \tag{20}$$

where r is the number of points in $N(T_0)$,

$$d_k = |\bar{T}_k - T_0|, \ \ k = 1 \quad \ldots, \ r \tag{21}$$

and $d_{\max}$ the distance of T_0 to the furthest point in $N(T_0)$:

$$d_{\max} = \max_{1 \le k \le r} d_k \tag{22}$$

The total weight of z_k becomes $\omega_k W_k$. In the loess smoother $N(T_0)$ consists of the r closest points to T_0, regardless of which side they are on. The span, λ, is defined by

$$\lambda = \frac{r}{K} \tag{23}$$

The span controls the smoothness of the fitted relationship. A small value of λ results in a relatively rough curve.

In Fig. 8, the nonparametric method is illustrated for the SW/W/NW category of Bern. The figure presents the loess smooth for $\lambda = 0.3$, 0.5 and 0.8. For the largest span the smooth approaches the linear regression fit. Furthermore, it should be noted that in this paper, some pre-smoothing has been done by averaging the precipitation values in each temperature class. Pre-smoothing is a common technique when one deals with huge amounts of data.

One purpose of smoothing is data description. Smooth curves help our eyes with the interpretation of a scatter plot and are useful for finding suitable parametric formulations. The nonparametric smoother also provides additional diagnostics to check the adequacy of the fitted models. The *QLR* statistic in the previous section can be used for that purpose:

$$QLR = D(\hat{\boldsymbol{\theta}}_0) - D(\lambda) \tag{24}$$

where $D(\lambda)$ is the deviance for the nonparametric fit. The expression for $D(\lambda)$ is identical to Eq. (16), except that the estimate of μ_k is now determined by λ rather than by estimated parameters. An effective number of parameters or degrees of freedom (*df*) for the nonparametric fit is needed in order to find the critical values of the test statistic. This effective number is mainly controlled by the span λ. The degrees of freedom, *df*, decrease as λ increases. Details about the computation of *df* can be found in Hastie and Tibshirani (1990). A value of the *AIC* statistic for the nonparametric fit can be obtained by replacing *q* in Eq. (18) by *df*. This statistic can be very helpful for finding a suitable span for the smoother.

The adequacy of a nonparametric fit can be tested with the scaled deviance $D(\lambda)$. This statistic has, under the null hypothesis, a chi-squared distribution with $K-df$ degrees of freedom.
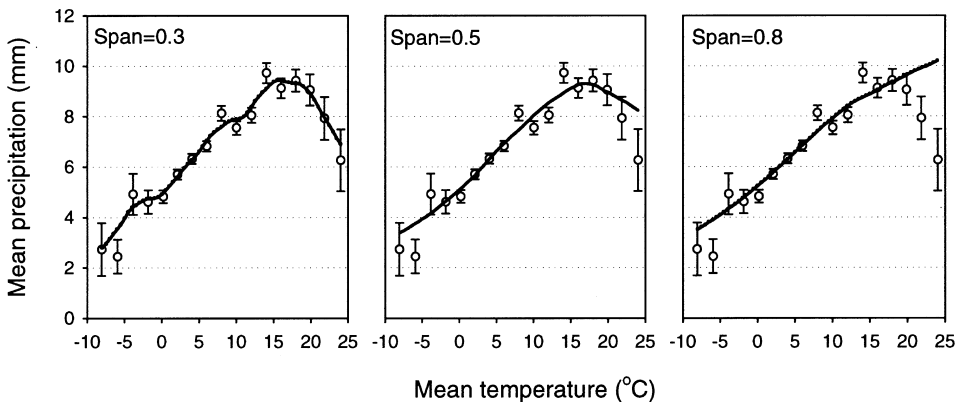

Fig. 8. Illustration of the nonparametric method for wet days at Bern for the SW/W/NW category (Fig. 5, right panel). The loess smooth is applied to the data for three values of the span, $\lambda = 0.3$, 0.5 and 0.8. The choice of $\lambda = 0.5$ in the middle panel resulted in the smallest value of the Akaike-information criterion.

3.3. Extension to two predictor variables

In Section 2.2 it was shown that the expected precipitation amount is influenced by the strength of the flow F. The dependence of P on both T and F can be described by a model similar to that for the P–T relationship:

$$P = \exp[g(T,F)] + \epsilon \tag{25}$$

where ϵ is a random error with zero mean. The change of the coefficient of variation with T and F is approximated by the linear relation:

$$CV = \alpha + \beta T + \gamma F \tag{26}$$

The function $g(T,F)$ and the coefficients α, β and γ in Eq. (26) are estimated for each category of flow direction (N/NE, E/SE/S and SW/W/NW) separately.

Parametric models with two predictor variables can be analysed in the same way as the P–T relationship in Section 3.1. There is a backfitting algorithm for nonparametric models. This iterative smoothing algorithm can be used when the predictor effects in $g(T,F)$ are additive. Eq. (25) then takes the form:

$$P = \exp[a + g_1(T) + g_2(F)] + \epsilon \tag{27}$$

where $g_1(T)$ and $g_2(F)$ are smooth functions in T and F, respectively. To avoid free constants in Eq. (27), it is assumed that $E[g_1(T)] = E[g_2(F)] = 0$. The iteration process is initialised with $\hat{g}_1(T) = \hat{g}_2(F) = 0$ and $\hat{a} = \ln(\bar{P})$, where $\bar{P}$ is the mean precipitation amount of all wet days. The backfitting algorithm replaces the weighted linear regression of the adjusted dependent variable on temperature and flow components by an additional loop in which $g_1(T)$ and $g_2(F)$ are estimated alternately by smoothing partial residuals, e.g. using the loess smoother in the previous section. Let z_k be the adjusted dependent variable for the kth class of the two predictor variables ($k = 1, \ldots, K$), and let $\bar{T}_k$ and $\bar{F}_k$ denote the mean temperature and strength of the flow, respectively, for this class. Using the current estimate of $g_2(F)$ an improved estimate of $g_1(T)$ is obtained by smoothing the partial residuals:

$$r_{1,k} = z_k - \hat{a} - \hat{g}_2(\bar{F}_k) \quad k = 1, \ldots, K \tag{28}$$

on T. With this new estimate we can get a revised estimate of $g_2(F)$ by smoothing the partial residuals:

$$r_{2,k} = z_k - \hat{a} - \hat{g}_1(\bar{T}_k) \quad k = 1, \ldots, K \tag{29}$$

on F. This process is continued until neither $g_1(T)$ nor $g_2(F)$ change from one iteration to the next.

4. Results

We now present the results of the regression of daily precipitation on temperature and strength of the flow. This regression needs information about the coefficient of variation CV. The parameters in the model for CV are, therefore, discussed first. We then present our nonparametric fits. These fits are used to find a suitable parametric model. Special attention is given to the screening of models for the Bern data.

4.1. Coefficient of variation CV

For each of the three stations, Bern, Neuchâtel and Payerne, the parameters in Eq. (26) were estimated for the three categories of flow direction using a weighted least-squares regression procedure with the number of wet days in a class specifying the weight. When one or two parameters were not significant at the 0.05 level, the model was fitted again with only the significant terms left. Table 2 presents the parameter estimates for the three stations. The table shows that for the SW/W/NW category, F cannot be neglected in the calculation of CV. Because the range for F is about 30 geostrophic flow units, the influence of F on CV can be, for Bern, as large as 0.58. The influence of T on CV is somewhat smaller. The range for T is roughly 25°C which, in the worst case, may affect the magnitude of CV by 0.24 (Bern, N/NE category).

4.2. Nonparametric fits

For each station and category of flow direction, we considered the nonparametric estimation of the functions $g_1(T)$ and $g_2(F)$ in Eq. (27). The spans λ_T and λ_F for T and F were allowed to vary between 0.1 and 1.0 with intervals of 0.1. For each combination of spans, we calculated the AIC. The combination of λ_T and λ_F that gave the smallest AIC was considered further. To facilitate the comparison between the stations, we decided to use, for all of them, the same span for a specific category of flow direction. This combination consisted of the lowest λ_T and λ_F of the three stations. For the three categories of flow direction, this resulted in the following combinations of spans: (1) N/NE: $\lambda_T = 0.4$, $\lambda_F = 0.5$; (2) E/SE/S: $\lambda_T = 0.7$, $\lambda_F = 0.9$; and (3) SW/W/NW: $\lambda_T = 0.4$, $\lambda_F = 0.5$.

Figs 9 and 10 present the estimated shapes of $g_1(T)$ and $g_2(F)$, respectively. From Fig. 9, it can be noted that there is, in general, an increase of $g_1(T)$ with increasing T. For the N/NE and SW/W/NW categories the increase of $g_1(T)$ with T is small for large values of T, though this effect is less pronounced than in Figs 2 and 5 where often a decrease in the mean precipitation amount with increasing T is found. For the SW/W/NW category, the graph for Neuchâtel is rather different from that for Bern and Payerne. It is also apparent that for the E/SE/S category $g_1(T)$ is almost linear.

Fig. 10 shows, for the SW/W/NW category, a strong increase of $g_2(F)$ with increasing F, which is in line with Fig. 6 for Bern. Possible explanations of this phenomenon are the enhanced supply of maritime air on days with a strong west circulation and a larger

Table 2
Estimates of the parameters in Eq. (26) for the coefficient of variation

Parameter	Bern			Neuchâtel			Payerne		
	N/NE	E/SE/S	SW/W/NW	N/NE	E/SE/S	SW/W/NW	N/NE	E/SE/S	SW/W/NW
α	1.0556	1.2198	1.2842	1.1074	1.2376	1.2386	1.2115	1.1736	1.2127
β	0.0097	—	−0.0081	0.0092	—	—	—	—	—
γ	—	—	−0.0193	—	—	−0.0180	−0.0083	—	−0.0128

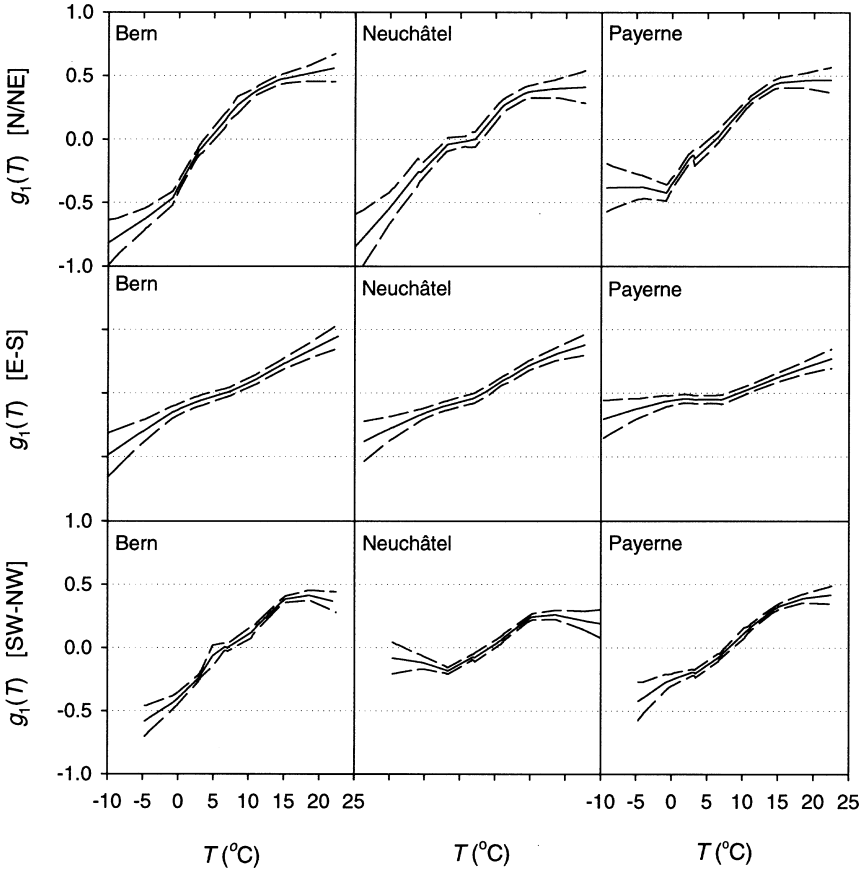The given estimates are significant at the 0.05 level.

Fig. 9. Estimates of the contribution $g_1(T)$ of temperature T to the logarithm of the expected daily precipitation amounts on wet days for Bern, Neuchâtel and Payerne, for three categories of flow direction. The dashed curves are, pointwise, standard-error bands (calculated according to Chambers and Hastie, 1993, pp. 303–304).

influence of the mountains on such days. However, $g_2(F)$ is almost constant at low values of F, especially for Neuchâtel and Payerne. For the N/NE category the relationship between P and F is weaker and more or less opposite to that for the SW/W/NW category. Besides, there are considerable differences between the three stations for the N/NE category (for small values of F there is a decrease of $g_2(F)$ with increasing F, for Bern $g_2(F)$ continues to decrease while especially for Neuchâtel $g_2(F)$ starts increasing for larger values of F). A reversal of the effect of the flow on orographic rainfall has been reported elsewhere (Weston and Roy, 1994; Brown, 1995). The differences between the stations indicate that the local topography is important. For the E/SE/S category the relationship between P and F is weak, which is probably caused by the fact that the stations are situated along the lee side of the Alps.

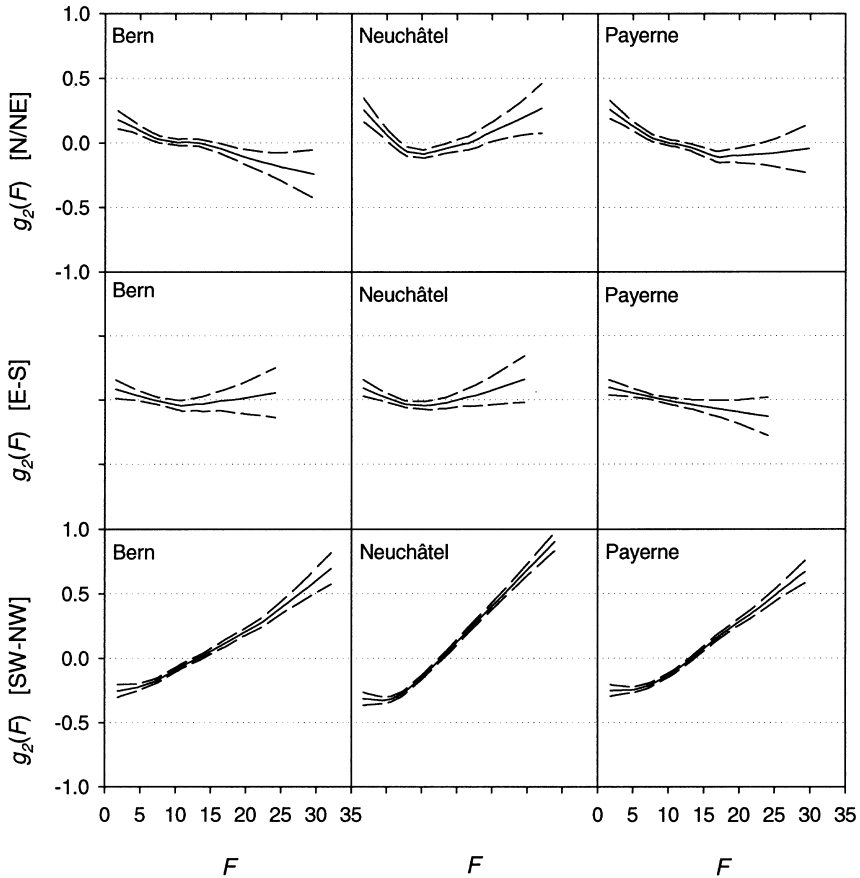It is important to combine the NW direction with the W and SW directions and not

Fig. 10. Estimates of the contribution $g_2(F)$ of strength of the flow F to the logarithm of the expected daily precipitation amounts on wet days for Bern, Neuchâtel and Payerne, for three categories of flow direction. The dashed curves are, pointwise, standard-error bands (Chambers and Hastie, 1993, pp. 303–304); flow units are geostrophic expressed as hPa per 10° latitude at 45°N (1 unit is equivalent to 0.87 m s^{-1}).

with the N and NE directions. There is a sharp transition in the effect of F on wet-day precipitation between the NW and N directions, causing large differences in the shape of $g_2(F)$ for the SW/W/NW and the N/NE categories.

4.3. Parameter estimates and goodness of fit

It appeared that an NCS with four knots was sufficient to model the non-linear effect of T. The position of the knots was found by trial and error. Only minor improvement could be achieved when the position of the knots was optimised for each station and category of flow direction. Therefore, we chose to locate the knots for T at the same positions for all stations and categories of flow direction at 2, 7, 12 and 17°C. We used a truncated linear term $(F - t_1)_+$ to represent the changes in the slope of the contribution of the strength of the

flow for the N/NE (Neuchâtel, Payerne) and SW/W/NW (all stations) categories. For the complete parametric model, the function $g(T,F)$ in Eq. (25) takes the form:

$$g(T,F) = a + bT + d_1(T - s_1)_+^3 + d_2(T - s_2)_+^3 + d_3(T - s_3)_+^3 + d_4(T - s_4)_+^3$$
$$+ e_1F + e_2(F - t_1)_+ \tag{30}$$

where $(s_1, \ldots, s_4) = (2, 7, 12, 17)$ and $t_1 = 7$ (SW/W/NW), 9 (N/NE, Neuchâtel) or 16 (N/NE, Payerne). Depending on the situation, a number of terms could be left out in the final model. For the E/SE/S category, the model even reduced to the simple linear model as given by Eq. (3). For the other two categories, we compared, for Bern, the final model with the linear model:

$$g(T,F) = a + bT + eF \tag{31}$$

Table 3 presents, for this station, the scaled deviances and the accompanying degrees of freedom for the two parametric models and the loess fits. The number of classes, K, equals 58, 47 and 60 for the N/NE, E/SE/S, and SW/W/NW categories, respectively. The deviances can be used for screening models.

For the N/NE and SW/W/NW categories, the deviances for the linear model are much larger than those for the loess model, indicating that the linear model is inadequate. However, for the E/SE/S category, the loess fit does not lead to a significant decrease of the deviance. This confirms the choice of the linear model for that category. For the N/NE category, the difference between the deviances for the nonparametric loess model and the final parametric NCS model is 8.1 on 4.7 *df*, which is not significant according to the chi-squared distribution. The two models thus, fit equally well. However, for the SW/W/NW category, the nonparametric fit is much better than that achieved with the final parametric NCS model. This is because an NCS with four knots is not capable of describing the rather wiggly shape of the function $g_1(T)$ in Fig. 9 for that category. We can improve the parametric fit by supplying two additional knots. In that case, the degrees of freedom of the loess model and the NCS model are nearly the same and the deviance of the NCS model (74.4) is even slightly smaller. Nevertheless, we decided to use the NCS model with four knots because we have no physical reasons to assume that the wiggly shape is real and also because the other two stations did not have the same problem with the SW/W/NW category. To assess the consequences of our decision, we performed the computations for Section 5 also with the NCS model with six knots.

The adequacy of the fit of the final model can be tested by comparing the scaled deviances in Table 3 with the percentiles of the chi-squared distribution. These values are significant at the 5% level for the N/NE and SW/W/NW categories. This is also the

Table 3
Scaled deviances and accompanying degrees of freedom (in parentheses) for the linear model, the loess fit and the NCS model for Bern

Model	N/NE	E/SE/S	SW/W/NW
Linear model	107.6 (55)	44.7 (45)	114.4 (57)
Loess model	69.1 (48.3)	41.5 (41.6)	74.8 (49.9)
NCS model	77.2 (53)	—	95.7 (55)

case for the loess fit for these categories. For the SW/W/NW category, a large contribution to the deviance statistic comes from classes with moderate temperatures and high values of F. This is of some concern because these classes have relatively high mean precipitation amounts and they refer to wet days at or near the border of the observed T–F range as given in Fig. 6. Both positive and negative outliers occur. There is, however, no clustering of large positive or negative residuals that may suggest a systematic model deficiency. The poor fit for the N/NE category is caused by a serious overestimation of the mean precipitation amount in a single class with low temperatures ($T < -4°C$) and weak flows ($2.5 < F < 5$). This outlier has a rather strong influence on the coefficient e_1 for the effect of F. The estimate of this coefficient increases by about 15% when the outlier is omitted.

The parameter estimates of the final model for the three stations and the three categories of flow direction are presented in Table 4. The estimates of a, b, d_1,…, d_4 in that table are not provided by the S-PLUS software. S-PLUS works with the B-spline basis functions in Eq. (7) instead of the truncated cubic polynomials in Eq. (5). For $q = 4$ knots, there is, however, no advantage in working with B-splines. The estimates of a, b, d_1,…, d_4 were obtained from the S-PLUS output by solving a set of six linear equations with six unknowns. The two parameter constraints in Eq. (6) give the first two equations and the values of μ at the four knots (with F set to zero) give the other four equations. The B-spline basis functions for T and the (piecewise) linear terms in F were statistically significant at the 5% level.

From Table 4, it is seen that there are marked differences between the various categories of flow direction. It was already obvious, from Fig. 10, that, in particular, the effect of F on P differs from category to category. There are also differences between the stations mutually, in particular between Bern and Payerne, on the one hand, and Neuchâtel on the other.

Table 4 also presents the scaled deviances for the fitted models. The large values for Neuchâtel for the N/NE and SW/W/NW categories are due to outliers that occur more or less at the same positions as those for Bern. For Payerne, there is no evidence of lack of fit.

5. Application to precipitation scenario production

The objective of the statistical linkage of daily precipitation to temperature and flow characteristics was to provide precipitation scenarios for hydrological impact studies. This application requires that the fitted relationships continue to hold under the altered climate. The application, furthermore, needs reasonable guesses of the changes in the predictor variables. One possibility is that the changes in the circulation patterns can be neglected, as in Matyasovszky et al. (1993), but that there is a homogeneous temperature rise over a large area. That this is indeed a realistic option for the changes owing to increased greenhouse gases in the atmosphere is illustrated in Fig. 11. The figure gives the changes in temperature and flow characteristics over Switzerland in a simulation with the Hadley Centre coupled ocean–atmosphere model (Mitchell et al., 1995). Both greenhouse gases and the direct radiative effects of sulphate aerosols are represented in this simulation

Table 4
Estimates of the coefficients in Eq. (30), the scaled deviances D and the degrees of freedom df

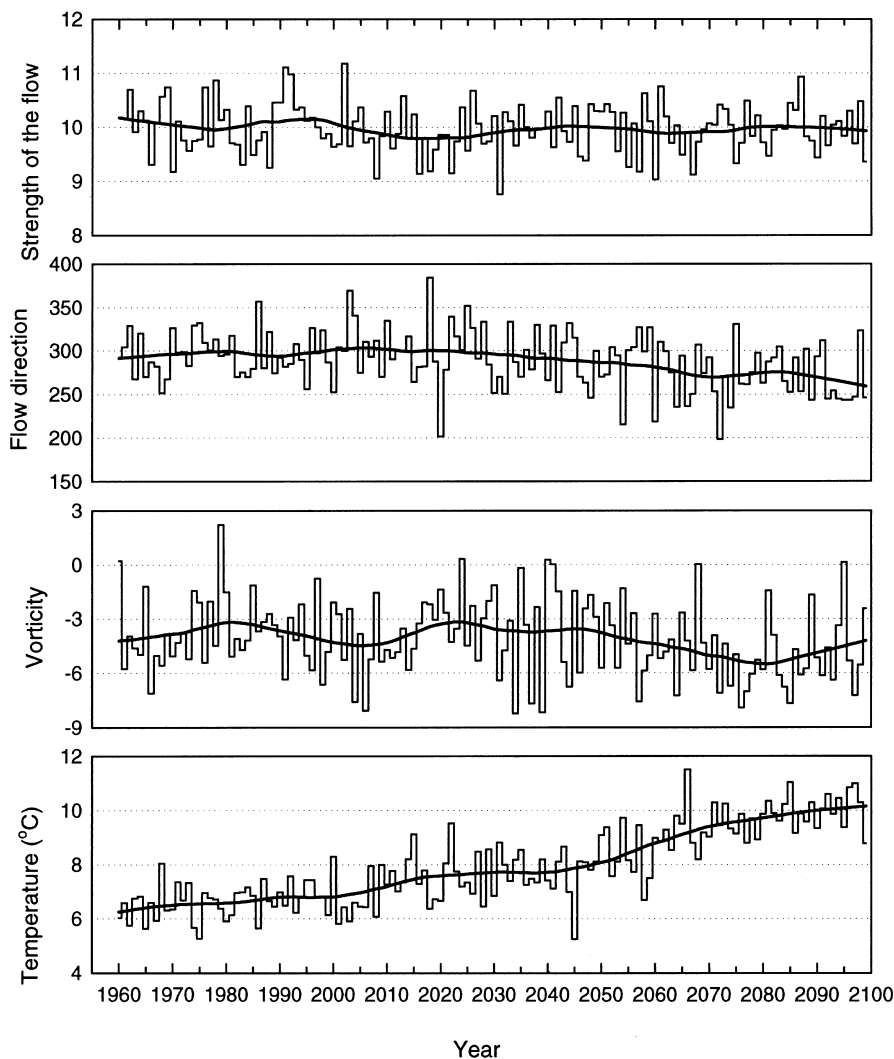|	Bern			Neuchâtel			Payerne		
	N/NE	E/SE/S	SW/W/NW	N/NE	E/SE/S	SW/W/NW	N/NE	E/SE/S	SW/W/NW
a	1.295571	1.501876	1.420118	1.455661	1.504057	1.589376	1.320072	1.645614	1.443434
b	0.071505	0.028126	0.047836	0.043234	0.027312	-0.004352	0.037504	0.017833	0.019988
d_1	-0.000088	—	0.000148	0.000151	—	0.000563	0.000390	—	0.000401
d_2	-0.000188	—	-0.000677	-0.000761	—	-0.001641	-0.001452	—	-0.001231
d_3	0.000640	—	0.000911	0.001067	—	0.001595	0.001734	—	0.001261
d_4	-0.000364	—	-0.000382	-0.000458	—	-0.000516	-0.000672	—	-0.000430
e_1	-0.014253	—	—	-0.059550	—	—	-0.022825	—	—
e_2	—	—	0.033974	0.085528	—	0.055670	0.026330	—	0.040701
D	77.2	44.7	95.7	101.8	44.3	85.0	57.7	32.4	57.3
df	53	45	55	51	44	52	50	45	54

Fig. 11. Annual mean values for temperature and flow characteristics over Switzerland in a simulation with the Hadley Centre coupled ocean–atmosphere model with aerosol effects included (Mitchell et al., 1995). Flow and vorticity units are geostrophic, expressed as hPa per 10° latitude at 45°N (1 unit is equivalent to 0.87 m s^{-1} and 0.78 × 10^{-6} s^{-1} for flow and vorticity, respectively). The solid lines are locally weighted running-line smooths with a span of 30 years.

experiment. Up to the year 2050, there are no changes in the annual averages of the direction and strength of the flow and the vorticity. On the other hand, the increase in temperature is quite clear. After the year 2050, there is a small decline in the vorticity and the mean flow direction tends to shift from north-westerly to westerly. The changes in flow direction mainly occur during the winter half of the year.

In this section, we first use the fitted parametric model for Bern to derive a precipitation

scenario for the case of a spatially homogeneous warming. Then we discuss the complications that arise if there are changes in the atmospheric flow as well. Some difficulties with the estimation of the temperature effect on precipitation are also identified.

5.1. Precipitation scenarios for the case of a spatially homogeneous warming

Here, we deal with the case in which there is a systematic change ΔT in the daily temperatures and there are no changes in the direction and strength of the flow. A quite reasonable assumption in this situation is that the number of wet days remains the same. For the sake of simplicity, we further assume that there is no seasonal variation in the values of ΔT. A precipitation scenario can then simply be obtained by multiplying the observed wet-day precipitation amounts by a scaling factor G. For a day with temperature T and strength of the flow F, G is derived as:

$$G(T, \Delta T) = \frac{\mu(T + \Delta T, F)}{\mu(T, F)} = \exp[g(T + \Delta T, F) - g(T, F)] \tag{32}$$

where $\mu(T,F)$ is the expected value of P as a function of T and F. Because in our models the effects of T and F on $g(T,F)$ are additive, G does not depend on F; for the linear model (E/SE/S category) G is even constant.

Fig. 12 presents G for the three categories of flow direction for $\Delta T = 1$ and $3°C$ using the parameter estimates for Bern in Table 4. The factor G for the E/SE/S category is rather different from that for the two other categories. For $\Delta T = 3°C$ the mean annual precipitation at Bern increases by 11.2% while the mean precipitation in the winter and summer half of the year increases by 16.8 and 7.5%, respectively.

A deterministic transformation of historical precipitation records implies that the temporal dependence of precipitation is more or less preserved as it should be when there are no significant changes in the atmospheric circulation. The transformation only requires a statistical description of the mean precipitation amounts instead of their complete distribution as in Matyasovszky et al. (1993). The method proposed by those authors also needs a substantial extension for applications where daily temperature data are needed.

5.2. Extensions for changes in the atmospheric flow

A scaling factor similar to that in Eq. (32) can be derived to account for the effect of a systematic change of F on the mean wet-day precipitation amounts. However, a simple transformation of the observed wet-day precipitation amounts is not sufficient for that case, because a change in the strength of the flow will generally be accompanied by an increase or decrease in the number of wet days. Klein Tank and Buishand (1995) describe the use of logistic regression to include or remove wet days in an observed record.

A deterministic transformation of observed rainfall is not the most obvious method when the frequencies of the flow directions change as well. In that case, it may be advantageous to combine a time series model for generating daily rainfall sequences, conditional on the large-scale circulation, with the regression models developed in the present paper, to adjust the precipitation amounts for the higher expected temperatures. The derivation of the temperature effect on the precipitation amounts needs some care in
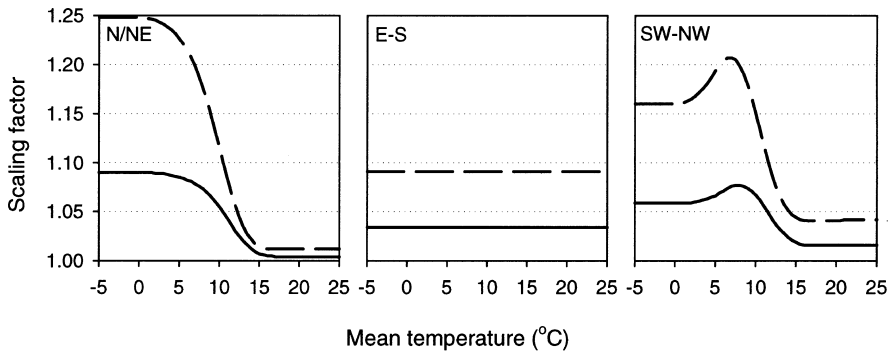
Fig. 12. Scaling factors, G, for Bern for the three categories of flow direction and for $\Delta T = 1$ (solid line) and 3°C (dashed line).

that application. Part of the temperature rise after the year 2050 in Fig. 11 is due to the systematic change in the mean flow direction. This contribution to the temperature rise must be separated from the overall warming resulting from the increased atmospheric greenhouse gas concentrations.

5.3. Confidence in the estimated temperature effect

The use of the transformation technique in Section 5.1 requires that the temperature effect on precipitation can be separated from other factors. Suitable climatic data for such a separation may not be available. Regression models with a limited number of parameters can only take the most important factors into account. However, a model with many predictor variables becomes intractable, in particular when the effects of these variables are non-linear.

There are also uncertainties in the modelling of the non-linear temperature effect on precipitation. In Section 4.3 we found that, for Bern, the parametric fit for the SW/W/NW category could be improved by taking an NCS with six knots for the temperature effect. The estimated change in summer precipitation is sensitive to the chosen NCS. For a spatially homogeneous warming of 3°C, the increase in the mean precipitation for the summer half of the year is only 4.1% for the NCS with six knots (was 7.5% for the NCS with four knots). Furthermore, the effect of this warming on the mean precipitation amounts at Neuchâtel and Payerne is smaller than that for Bern, especially in the winter half of the year (increases of 9.5% for Neuchâtel, 12.7% for Payerne and 16.8% for Bern). Although the temperature effect on precipitation may vary over the region, the differences may also be due to simplifications in our approach.

The negligence of seasonal variation in the model parameters and the scaling factor G, further lowers the confidence in the estimated temperature effect on precipitation. Another point of concern is that, at high temperatures, the change in the mean wet-day precipitation amounts with increasing temperature is much smaller than that expected for summer thunder storms (Klein Tank and Können, 1994). To get a better description of the $P–T$ relationship at high temperatures, it might be necessary to include some information about

the precipitation mechanism. This may also improve the reproduction of the annual cycle of the mean wet-day precipitation amounts.

6. Conclusions

In this paper, we explored the P–T relationship as a basis for precipitation scenario production. Three Swiss stations were considered: Bern, Neuchâtel and Payerne. For these stations, we included information about the direction and strength of the atmospheric flow F. An iterative smoothing technique gave a clear insight into the effects of T and F on the expected precipitation amounts on wet days. Parametric NCS were introduced as flexible tools to model the nonlinearities in the P–T relationships. Abrupt changes in the effect of F could be modelled by a truncated linear term. From the fitted relationships, a scaling factor was derived to produce a precipitation scenario for the case of a systematic temperature change. A combination with other models is necessary to use our relationships for the wet-day precipitation amounts in situations where the temperature increase is accompanied by a systematic change in the airflow. Information about the precipitation mechanism may be required to improve our estimates of the changes in precipitation, especially at high temperatures.

Acknowledgements

References

Bárdossy, A., Plate, E.J., 1992. Space–time model for daily rainfall using atmospheric circulation patterns. Water Resources Research 28, 1247–1259.

Brown, K.R., 1995. The effect of wind speed on orographic enhancement. Weather 50, 266–272.

Buishand, T.A., Klein Tank, A.M.G., 1996. Regression model for generating time series of daily precipitation amounts for climate change impact studies. Stochastic Hydrology and Hydraulics 10, 87–106.

Burlando, P., Rosso, R., 1991. Extreme storm rainfall and climatic change. Atmospheric Research 27, 169–189.

Chambers, J.M., Hastie, T.J., 1993. Statistical Models in S. Chapman and Hall, London, 608 pp.

Clarke, R.T., 1994. Statistical Modelling in Hydrology. Wiley, Chichester, 412 pp.

Cleveland, W.S., 1979. Robust locally weighted regression and smoothing scatterplots. Journal of the American Statistical Association 74, 829–836.

Cole, J.A., Slade, S., Jones, P.D., Gregory, J.M., 1991. Reliable yield of reservoirs and possible effects of climatic change. Hydrological Sciences Journal 36, 579–598.

Giorgi, F., Shields Brodeur, C., Bates, G.T., 1994. Regional climate change scenarios over the United States produced with a nested regional climate model. Journal of Climate 7, 375–399.

Greville, T.N.E., 1969. Introduction to spline functions. In: Greville, T.N.E. (Ed.), Theory and Applications of Spline Functions. Academic Press, New York, pp. 1–35.

Hastie, T.J., Tibshirani, R.J., 1990. Generalized Additive Models. Chapman and Hall, London, 335 pp.

Hughes, J.P., Lettenmaier, D.P., Guttorp, P., 1993. A stochastic approach for assessing the effect of changes in synoptic circulation patterns on gauge precipitation. Water Resources Research 29, 3303–3315.

Jones, P.D., Hulme, M., Briffa, K.R., 1993. A comparison of Lamb circulation types with an objective classification scheme. International Journal of Climatology 13, 655–663.

Jones, R.G., Murphy, J.M., Noguer, M., 1995. Simulation of climate change over Europe using a nested regional-climate model. Part I: assessment of control climate, including sensitivity to location of lateral boundaries. Quarterly Journal of the Royal Meteorological Society 121, 1413–1449.

Kattenberg, A., Giorgi, F., Grassl, H., Meehl, G.A., Mitchell, J.F.B., Stouffer, R.J., Tokioka, T., Weaver, A.J., Wigley, T.M.L., 1996. Climate models-projections of future climate. In: Houghton, J.T., Meira Filho, L.G., Callander, B.A., Harris, N., Kattenberg, A., Maskell, K. (Eds.), Climate Change 1995: The Science of Climate Change, Contribution of Working Group I to the Second Assessment Report of the Intergovernmental Panel on Climate Change. Cambridge University Press, Cambridge, UK, pp. 285–357.

Klein Tank, A.M.G., Buishand, T.A., 1993. Modelling daily precipitation as a function of temperature for climate change impact studies. Scientific Report WR-93-02. KNMI, De Bilt, 34 pp.

Klein Tank, A.M.G., Buishand, T.A., 1995. Transformation of precipitation time series for climate change impact studies. Scientific Report WR-95-01. KNMI, De Bilt, 63 pp.

Klein Tank, A.M.G., Können, G.P., 1994. The dependence of daily precipitation on temperature. In: Proceedings of the 18th Annual Climate Diagnostics Workshop, Boulder, Colorado, 1–5 November 1993, pp. 207–211.

Matyasovszky, I., Bogárdi, I., Bárdossy, A., Duckstein, L., 1993. Space–time precipitation reflecting climate change. Hydrological Sciences Journal 38, 539–558.

McCullagh, P., 1986. Quasi-likelihood functions. In: Kotz, S., Johnson, N.L., Read, C.B. (Eds.), Encyclopedia of Statistical Sciences, vol. 7. Wiley, New York, pp. 464–466.

McCullagh, P., Nelder, J.A., 1989. Generalized Linear Models, 2nd edn. Chapman and Hall, London, 511 pp.

Mitchell, J.F.B., Johns, T.C., Gregory, J.M., Tett, S.F.B., 1995. Climate response to increasing levels of green-house gases and sulphate aerosols. Nature 376, 501–504.

Schüepp, M., Schirmer, H., 1977. Climates of central Europe. In: Wallén, C.C. (Ed.), World Survey of Climatology, vol. 6. Elsevier, Amsterdam, pp. 3–73.

Weston, K.J., Roy, M.G., 1994. The directional-dependence of the enhancement of rainfall over complex orography. Meteorological Applications 1, 267–275.

Wilks, D.S., 1992. Adapting stochastic weather generation algorithms for climate change studies. Climatic Change 22, 67–84.

Zorita, E., Hughes, J.P., Lettenmaier, D.P., von Storch, H., 1995. Stochastic characterization of regional circulation patterns for climate model diagnosis and estimation of local precipitation. Journal of Climate 8, 1023–1042.